WEP Warwick Evans Publishing

International Journal of Materials Science and Technology Studies

ISSN: 3006-7693 (Print), ISSN: 3006-3744 (Online) | Volume 5, Number 3, Year 2026
DOI: https://doi.org/10.62051/ijmsts.v5n3.02
Journal homepage: https://wepub.org/index.php/IJMSTS/index

Preparation and Properties of ZnS/SnO_2 Composite Photocatalyst

Boji Wang, Hari Bala *

Henan Polytechnic University, Jiaozuo, China
*Corresponding Author

ABSTRACT

In this paper, ZnS/SnO_2 composite photocatalysts with different molar ratios were prepared by a two-step hydrothermal method. The influence of ZnS composite ratio on the material structure, morphology, optical properties and photocatalytic performance was systematically investigated. XRD and XPS results indicate that the SnO precursor is completely transformed into rutile SnO_2 during the hydrothermal process, and ZnS is composited on the SnO_2 surface in the form of cubic sphalerite, forming a heterostructure rather than a solid solution. SEM, TEM and EDS show that the composite exhibits a porous nano-aggregate morphology with a close heterojunction interface formed between ZnS and SnO_2. BET analysis reveals that the material possesses a mesoporous structure with a specific surface area of 14.36 m^2/g. UV-vis absorption spectra show that the absorption edge of the composite is red-shifted, extending the photoresponse range to the visible region. The photocatalytic degradation experiments of rhodamine B (RhB) demonstrate that the composite with a ZnS ratio of 80% (0.8-ZnS/SnO_2) exhibits the best performance, achieving a degradation rate of 93.52% within 70 min and a reaction rate constant of 3.74×10^{-2} min^{-1}, which is about 5 times that of commercial P25. Cyclic catalytic tests prove that the composite has good reusability and photostability. This study provides a feasible synthesis strategy and structural optimization basis for constructing efficient type II heterojunction photocatalysts.

KEYWORDS

ZnS; SnO_2; Composite photocatalyst; Heterojunction

1. INTRODUCTION

With the rapid development of industrialization and urbanization, organic dyes and other pollutants pose an increasing threat to the water environment. Photocatalysis technology, which can degrade organic pollutants using solar energy under ambient conditions, is considered a green and efficient environmental remediation approach. Among various photocatalytic materials, SnO_2 and ZnS have attracted widespread attention due to their good chemical stability [1], suitable band positions and low toxicity [2, 3]. However, single-component photocatalysts often suffer from high recombination rate of photogenerated electron–hole pairs and poor visible-light response [4, 5], limiting their practical application.

Constructing heterojunctions is one of the effective strategies to enhance photocatalytic efficiency [6, 7]. By combining two semiconductors with matched band positions, a built-in electric field is formed at the interface, promoting spatial separation of photogenerated carriers, thereby prolonging their lifetime and improving surface reaction efficiency [8]. SnO_2, an n-type wide-bandgap semiconductor (~3.6 eV), has excellent electron mobility, but its photoresponse is mainly concentrated in the UV region [9]. ZnS is also a wide-bandgap semiconductor (~3.7 eV) with a relatively negative conduction

band position and strong reduction ability [10]. Combining ZnS with SnO_2 to form a type II heterojunction theoretically enables directional electron transfer from ZnS to SnO_2 and hole transfer in the opposite direction, thus effectively suppressing carrier recombination [11, 12].

At present, studies on ZnS/SnO_2 composite photocatalysts are still relatively limited, especially regarding the systematic influence of the ZnS composite ratio on material structure and performance. In this paper, ZnS/SnO_2 composites with different ZnS contents are synthesized by a hydrothermal method. Various characterization techniques are employed to analyze the phase, morphology, surface chemical state, specific surface area and optical properties, and the photocatalytic activity is evaluated using RhB as a model pollutant. The optimal composite ratio is determined and the catalytic enhancement mechanism is discussed. This study provides an experimental basis and theoretical reference for developing efficient and stable heterojunction photocatalysts.

2. EXPERIMENTAL

Preparation of SnO precursorSnO powder was prepared by a hydrothermal method. 1.6 g of urea (CH_4N_2O) was dissolved in a mixed solvent system consisting of 96 mL ethanol and 224 mL deionized water, and stirred thoroughly until completely dissolved. Then, 1.444 g of $SnCl_2 \cdot 2H_2O$ was added to the above solution, and stirring was continued to form a uniform suspension. 6 M NaOH solution was added dropwise to adjust the pH to 11, followed by stirring for another 20 min to ensure full homogenization. The resulting mixed solution was transferred into a Teflon-lined stainless steel autoclave and kept at 160 °C for 26 h. After the reaction, the autoclave was naturally cooled to room temperature. The product was washed several times alternately with ethanol and deionized water to remove residual ions, then collected and dried in an oven at 60 °C for 8 h. After grinding, SnO precursor powder was obtained.

ZnS/SnO_2 composites were prepared by a hydrothermal method. 1 mmol $ZnCl_2$ and 1 mmol thiourea (CN_2H_4S) were added to 20 mL deionized water and stirred for 30 min to form a homogeneous solution. Subsequently, the pre-prepared SnO powder was added into the above solution at a Zn:Sn molar ratio of 4:5 (i.e., 0.8), which had been determined as the optimal synthesis ratio through a series of comparative experiments. After stirring for another 30 min, the mixed solution was transferred into a Teflon-lined autoclave and kept at 180°Cfor 24 h. After natural cooling to room temperature, the precipitate was repeatedly washed with ethanol and deionized water, then dried at 60°C for 8 h to obtain the 0.8-ZnS/SnO_2 sample ("0.8" denotes Zn:Sn atomic ratio = 4:5). To systematically investigate the effect of ZnS proportion, 0.4-ZnS/SnO_2, 0.6-ZnS/SnO_2 and 1.0-ZnS/SnO_2 were also synthesized as control samples using the same method.

3. RESULTS AND DISCUSSION

3.1. Phase Analysis

To systematically investigate the influence of ZnS composite ratio on the crystal structure of ZnS/SnO_2 composites, XRD measurements were performed on samples with ZnS proportions of 40%, 60%, 80% and 100%. The results are shown in Fig. 1.

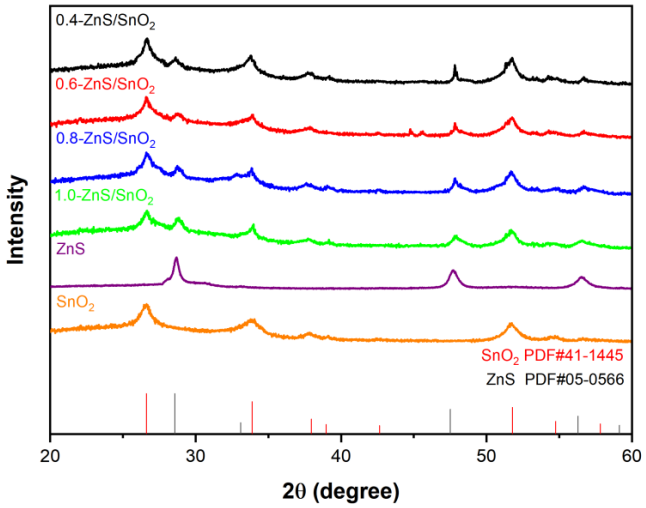

Figure 1. XRD patterns of SnO_2, ZnS, and ZnS/SnO_2 composites with different ZnS ratios

As the ZnS molar ratio increased from 0.4 to 1.0, the XRD patterns show a regular evolution: the characteristic diffraction peaks of ZnS monotonically increase with increasing ZnS loading, quantitatively reflecting the systematic change of ZnS phase mass fraction in each sample. Notably, when the ZnS content is too high, the SnO_2 characteristic peaks become relatively weakened. This is not due to an intrinsic decrease in SnO_2 crystallinity, but rather to the partial covering effect of excess ZnS nanoparticles on the SnO_2 surface, further confirming the heteroepitaxial growth of ZnS particles on the SnO_2 support surface.

Figure 1 also presents the comparative XRD patterns of SnO_2, pure ZnS, and the 0.8-ZnS/SnO_2 composite. Through systematic comparison with standard PDF cards, the phases can be clearly identified: the SnO_2 phase belongs to the tetragonal rutile system (PDF#41-1445), with characteristic diffraction peaks corresponding to (110), (101), (211) planes; the ZnS phase belongs to the cubic sphalerite system (PDF#05-0566), with peaks corresponding to (111), (220), (311) planes. The simultaneous presence of characteristic peaks of both phases with no obvious shift confirms that ZnS and SnO_2 form a physically composite heterostructure rather than a solid solution, with each phase maintaining its independent crystal integrity. Most importantly, the complete disappearance of SnO characteristic diffraction peaks in the composite XRD pattern strongly proves that the SnO precursor undergoes a complete phase transformation during the hydrothermal process, converting entirely to SnO_2. In addition, the broadened full width at half maximum of the diffraction peaks suggests that the material is within the nanometer scale, which is beneficial for providing a larger specific surface area and more surface active sites, offering sufficient reaction interfaces for photocatalytic reactions.

3.2. Microstructural Analysis

To deeply investigate the microstructural features of the ZnS/SnO_2 composite, systematic SEM, TEM and HRTEM characterizations were carried out, and the results are shown in Fig. 2.

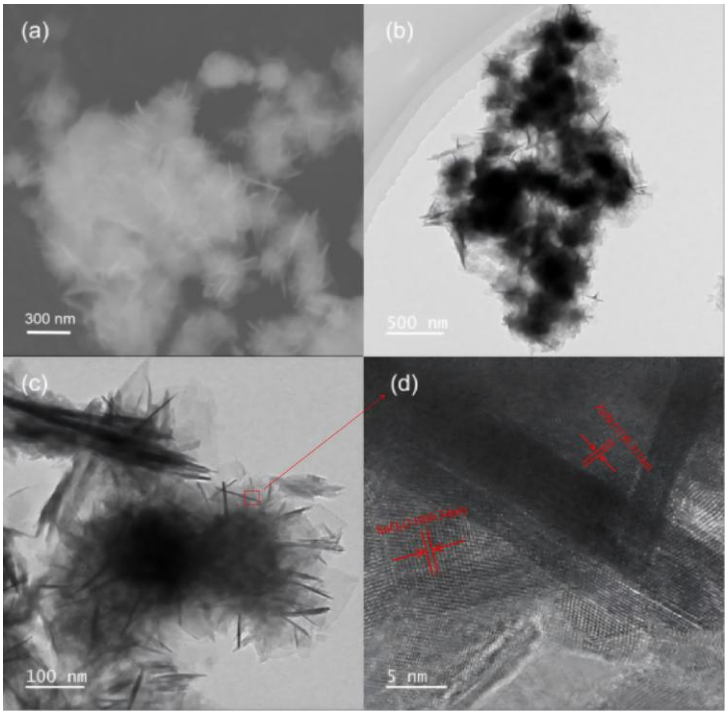

Figure 2. (a) SEM image of ZnS/SnO_2 composite, (b) and (c) TEM images, (d) HRTEM image

The SEM image shows that the composite presents a porous nano-aggregate morphology. This hierarchical porous structure originates from the directional aggregation growth of nanoparticles during the hydrothermal process, which is conducive to the diffusion and mass transfer of reactant molecules to active sites. In the HRTEM image, two distinct sets of lattice fringes with different spacings and their periodicity confirm that both ZnS and SnO_2 phases have good crystallinity. SnO_2 nanoparticles provide a high-surface-area reaction site and are anchored on the ZnS surface, forming a close heterojunction contact interface. The obvious lattice matching region in the composite structure is the microscopic structural basis for efficient charge transfer at the heterojunction. The coexistence of the two characteristic lattice spacings effectively rules out the possibility of a single-phase solid solution, confirming from the high-resolution morphology level the successful construction of a ZnS/SnO_2 two-phase heterostructure.

The energy-dispersive X-ray spectroscopy (EDS) elemental mapping verifies the structural uniformity of the composite from the chemical composition dimension, as shown in Fig. 3. The spatial distribution of Zn, S, Sn and O reveals: the co-localization of Zn and S confirms the formation and spatial distribution of the ZnS phase; the co-localization of Sn and O confirms the existence and dispersion state of the SnO_2 phase; the spatial overlap of the four elements reflects the intimacy of the heterojunction interface contact; the elemental distribution uniformity characterizes the reproducibility and compositional homogeneity of the synthesis method. The uniform elemental distribution indicates that during the hydrothermal synthesis, ZnS achieves highly dispersed in-situ growth on the SnO_2 surface, rather than simple physical mixing, which is of decisive structural significance for forming a type II heterojunction interface with efficient carrier transfer capability.

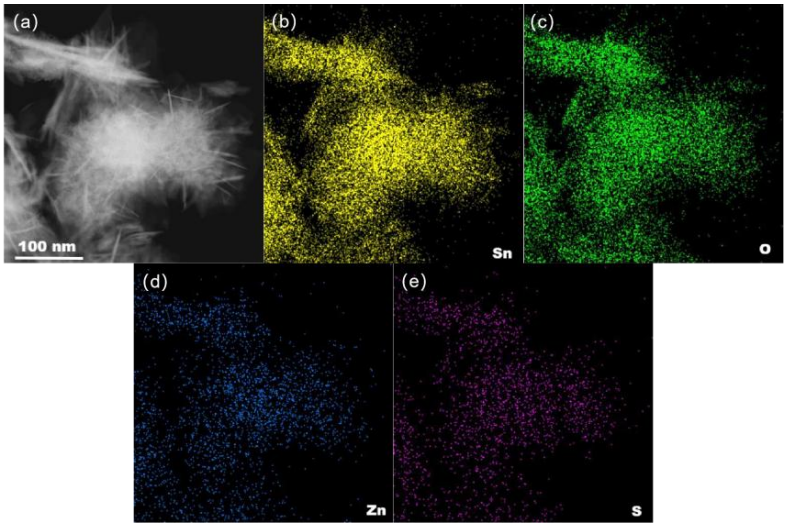

Figure 3. (a) Dark-field TEM image and elemental mapping of ZnS/SnO_2 composite: (b) Sn, (c) O, (d) Zn, (e) S

3.3. Specific Surface Area And Pore Structure Analysis

To explore the structural effects of the synthesized material, the specific surface area and pore size distribution were investigated using BET and BJH methods from nitrogen adsorption-desorption isotherms, as shown in Fig. 4. According to the IUPAC classification and isotherm type definitions, the N_2 adsorption-desorption isotherm of the prepared ZnS/SnO_2 composite belongs to type IV with an H3 or H4 hysteresis loop, characteristic of mesoporous materials, indicating the presence of a complex porous structure on the material surface.

The specific surface area of the ZnS/SnO_2 composite calculated by the BET method is 14.3551 m^2/g, the pore volume is 0.083 cm^3/g, and the average pore diameter is 22.058 nm.

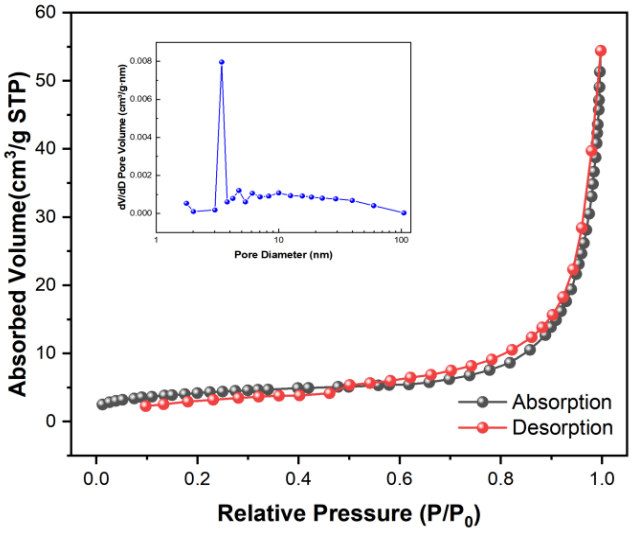

Figure 4. N_2 adsorption-desorption isotherm of ZnS/SnO_2 composite

The above pore structure parameters have important photocatalytic significance: the large specific surface area provides abundant surface active sites for photocatalytic reactions, significantly increasing the effective collision probability between the catalyst and substrate molecules; the existence of mesoporous channels facilitates the diffusion and mass transfer of organic pollutant molecules such as RhB to the internal active sites of the catalyst; the large pore space characterized by the pore volume quantitatively corresponds to the obvious adsorption enrichment behavior observed during the dark reaction stage of the photocatalytic degradation experiment, confirming the

physical pre-enrichment adsorption capacity of the material and constituting the structural basis for an adsorption-catalysis synergistic enhancement mechanism.

3.4. X-ray Photoelectron Spectroscopy (XPS) Analysis

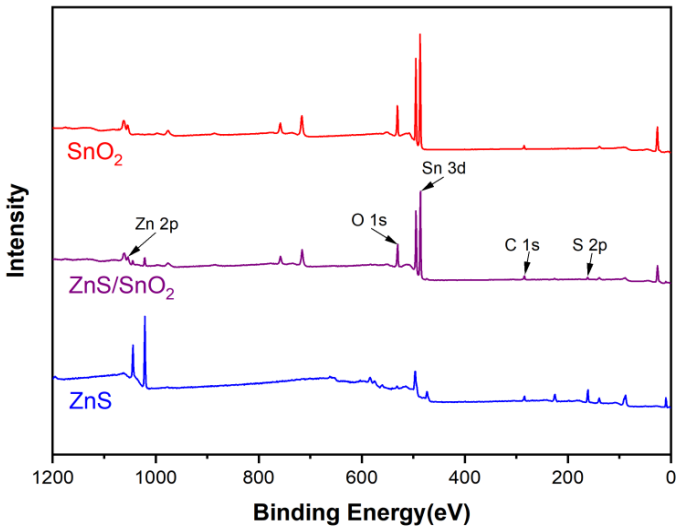

Figure 5. XPS survey spectrum of ZnS/SnO_2 composite

To determine the surface chemical composition of the synthesized product, XPS analysis was performed. Figures 5 and 6 show the survey spectrum and high-resolution fine spectra of each element for the ZnS/SnO_2 composite. The survey spectrum detects characteristic photoelectron peaks of five elements: Sn, O, Zn, S and C (the carbon signal originates from atmospheric carbon adsorbed on the sample surface or contaminant carbon used for binding energy calibration, C 1s = 284.8 eV). No other impurity element signals are detected, confirming that the elemental composition of the composite is consistent with the design.

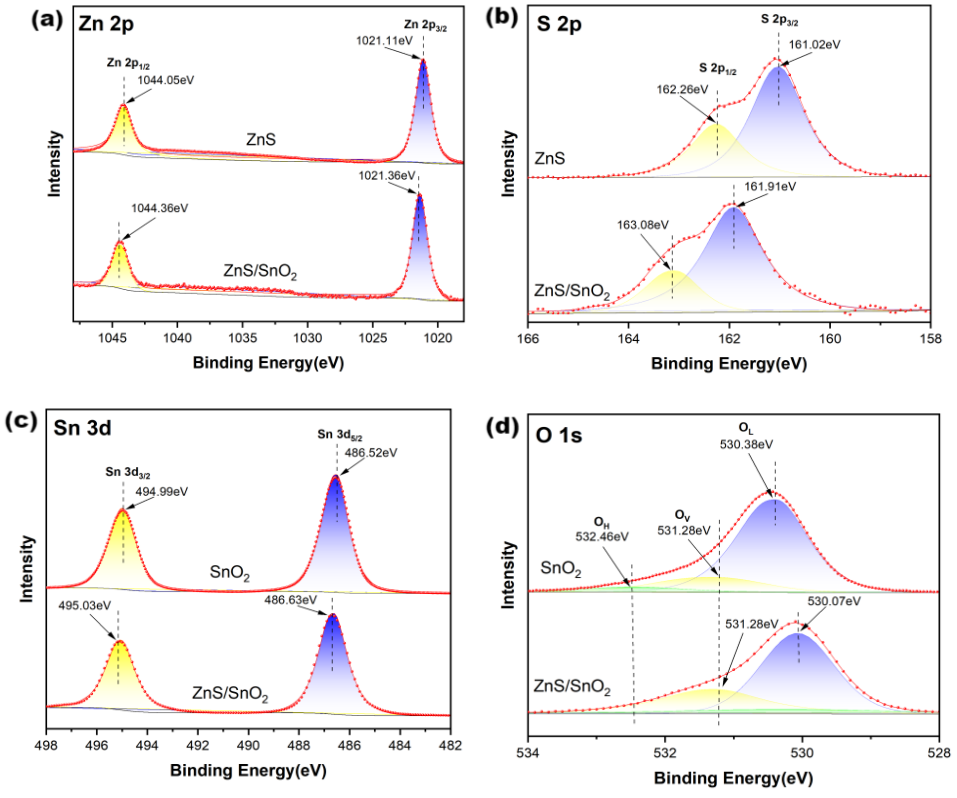

Figure 6. High-resolution XPS spectra of each element in ZnS/SnO2 composite

In Fig. 6, the Sn 3d orbital exhibits spin-orbit splitting into Sn $3d_{5/2}$ and Sn $3d_{3/2}$ characteristic peaks. Their binding energy positions and peak separation (~8.4 eV) are key to determining the chemical valence state of Sn: Sn $3d_{5/2}$≈486.5 eV corresponds to Sn^{4+} (SnO_2), excluding the presence of Sn^{2+} (SnO), confirming that SnO is completely oxidized to SnO_2 during the hydrothermal process. For the Zn 2p fine spectrum, the peak positions of Zn $2p_{1/2}$ and Zn $2p_{3/2}$ and their splitting energy (~23 eV) reveal the chemical environment of Zn: Zn $2p_{3/2}$ ≈ 1021.4 eV corresponds to Zn-S bonding in ZnS, and the symmetry of the peak shape indicates a uniform chemical environment of Zn with no interference from impurities such as ZnO. In the S 2p fine spectrum, the S 2p orbital splits into S $2p_{3/2}$ and S $2p_{1/2}$ (separation ~1.2 eV). The binding energy position is key to distinguishing ZnS from surface oxidized sulfur species: S $2p_{3/2}$ ≈ 161.5 eV corresponds to S^{2-} species in ZnS; if a peak near ~168 eV exists, it indicates surface sulfate (SO_4^{2-}) etc., suggesting slight oxidation. The O 1s fine spectrum and the catalytic significance of surface hydroxyl groups: the O 1s fine spectrum can usually be fitted into several sub-peaks; the presence of surface hydroxyl groups (precursors of •OH) has profound significance for the photocatalytic mechanism – under illumination, valence band holes (h^+) can oxidize surface -OH to strongly oxidizing hydroxyl radicals (•OH), which are one of the main reactive oxygen species for RhB degradation.

From the perspective of interfacial charge transfer analysis, the key information to focus on is the shift of binding energies of each element in the composite relative to their respective pure phases. In the ZnS/SnO_2 composite, the Sn 3d peak shifts to lower binding energy compared to pure SnO_2, while the Zn 2p peak shifts to higher binding energy compared to pure ZnS. This "one down, one up" symmetric binding energy change pattern can serve as spectroscopic evidence for directional electron transfer from the ZnS side to the SnO_2 side: the inflow of electrons increases the electron density around Sn atoms on the SnO_2 surface, enhancing the screening effect and making core-level electrons easier to excite, manifesting as a decrease in binding energy; conversely, the outflow of electrons decreases the electron density around Zn atoms on the ZnS surface, making core-level electrons harder to excite, resulting in an increase in binding energy. This interfacial charge transfer direction is fully consistent with the thermodynamic prediction of conduction band electron migration from the higher position (ZnS) to the lower position (SnO_2) in the type II heterojunction mechanism.

3.5. Optical properties and photoelectrochemical characteristics

To study the optical properties of the composite for optical performance characterization, UV-vis absorption spectroscopy, steady-state photoluminescence (PL) and time-resolved photoluminescence (TRPL) measurements were carried out, as shown in Fig. 7.

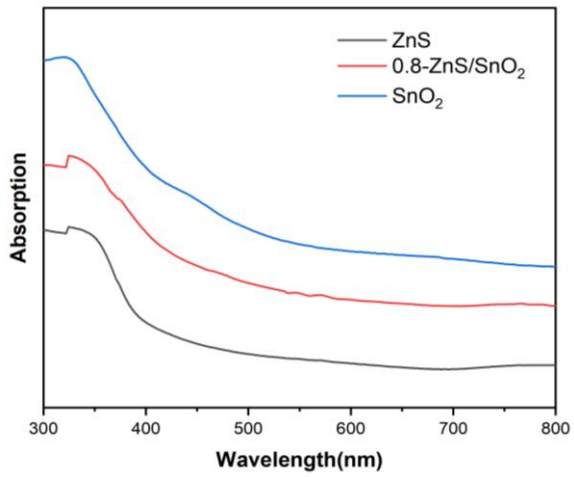

Figure 7. UV-vis absorption spectra of SnO_2, ZnS and 0.8-ZnS/SnO_2 composite

As shown in Fig. 7, using a UV-vis diffuse reflectance spectrometer with $BaSO_4$ as the reference, the absorption spectra of the prepared ZnS, SnO_2 and 0.8-ZnS/SnO_2 composite powder samples were

measured. The UV-vis absorption spectra reveal the photoresponse range and electronic transition characteristics of the composite. Compared to pure SnO_2 (band gap ~3.6 eV, absorption edge ~344 nm) and pure ZnS (band gap ~3.7 eV, absorption edge ~335 nm), the absorption edge of the 0.8-ZnS/SnO_2 composite is significantly red-shifted, extending into the visible region. This phenomenon can be explained by the following mechanisms: band bending effect – the built-in electric field at the heterojunction interface changes the local band structure; defect state introduction – surface defects (such as sulfur vacancies, oxygen vacancies) generated during hydrothermal synthesis introduce sub-gap states within the band gap, expanding the light absorption range.

3.6. Photocatalytic Activity Evaluation

Rhodamine B (RhB) aqueous solution was used as a model pollutant to systematically evaluate the photocatalytic degradation performance of the 0.8-ZnS/SnO_2 composite under simulated solar irradiation, as shown in Fig. 8. During the dark reaction stage (−15 min to 0 min), the RhB solution concentration decreases significantly, indicating that the composite has a remarkable physical adsorption pre-enrichment ability, which quantitatively corresponds to the large pore volume and specific surface area parameters from BET measurements, confirming the effectiveness of the adsorption-catalysis synergistic enhancement mechanism. As the photocatalytic reaction proceeds, the characteristic absorption peak intensity of RhB at 554 nm rapidly attenuates, while the absorption peak position shifts to shorter wavelengths (blue shift), revealing the dual pathway of RhB degradation: the blue shift corresponds to the stepwise N-deethylation degradation sequence of the RhB chromophore (RhB → N,N,N'-triethylrhodamine → ... → rhodamine), while the continuous attenuation of peak intensity corresponds to the direct oxidative ring-opening mineralization of the xanthene conjugated system. At the later stage of the catalytic reaction, the absorption peak at 554 nm tends to disappear, but residual absorption from secondary organic products still exists, indicating that under the present experimental conditions, efficient degradation of the organic pollutant is achieved, but complete mineralization is not yet reached, providing a clear direction for further performance optimization of ternary systems.

To compare the actual influence of different ZnS ratios in the composite on the photocatalytic degradation of RhB, comparative tests were performed on n-ZnS/SnO_2 samples with different ZnS contents, and the most suitable ratio was selected. Figure 9 shows the plots of C_t/C_0 versus time and the corresponding $\ln(C_t/C_0)$ versus time for RhB solutions over composites with different ZnS contents. Figure 9(a) clearly shows the influence of different ZnS contents on the system; it is evident that 0.8-ZnS/SnO_2 exhibits the best catalytic rate, with a degradation rate of 83.66% within 40 min and 93.52% within 70 min. To further compare the reaction rates, pseudo-first-order kinetics fitting ($\ln(C_t/C_0) = kt$) was performed, where the slope k represents the reaction rate constant. From Fig. 9(b), for ZnS contents of 40%, 60%, 80% and 100%, the reaction rate constants are 7.04×10^{-3}, 7.86×10^{-3}, 3.74×10^{-2} and 1.08×10^{-2} min^{-1}, respectively. It is evident that the ZnS content of 80% is the best among the samples, thus determining that 80% ZnS composite is the optimal ratio.

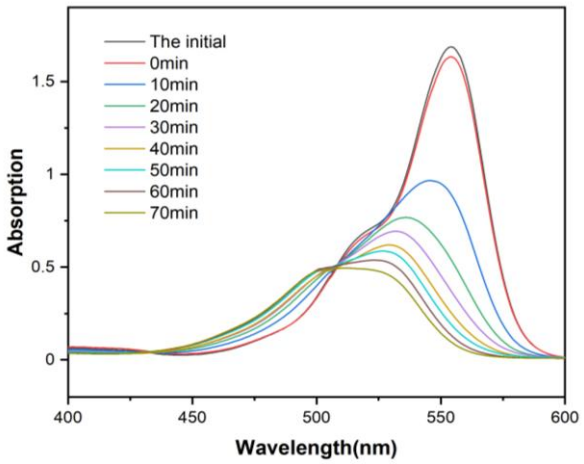

Figure 8. UV-vis absorption spectra of RhB degradation by 0.8-ZnS/SnO_2 composite

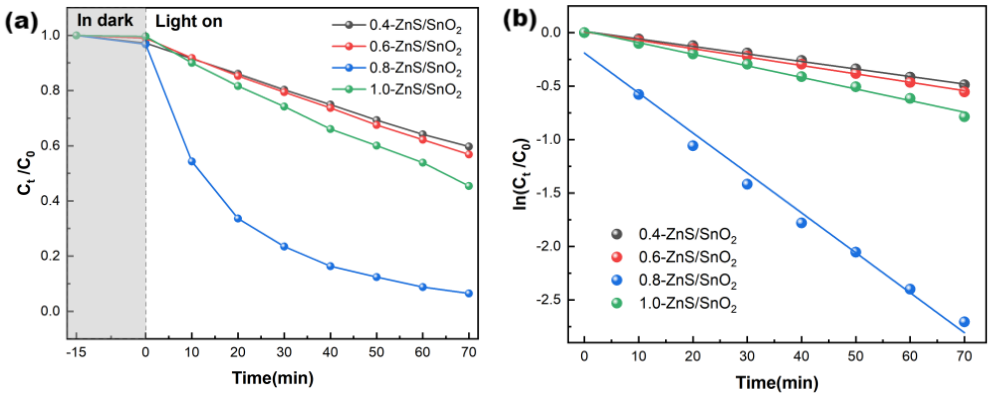

Figure 9. (a) C_t/C_0 vs. time plots for photocatalytic degradation of RhB over ZnS/SnO_2 composites with different ZnS ratios; (b) ln(C_t/C_0) vs. time plots

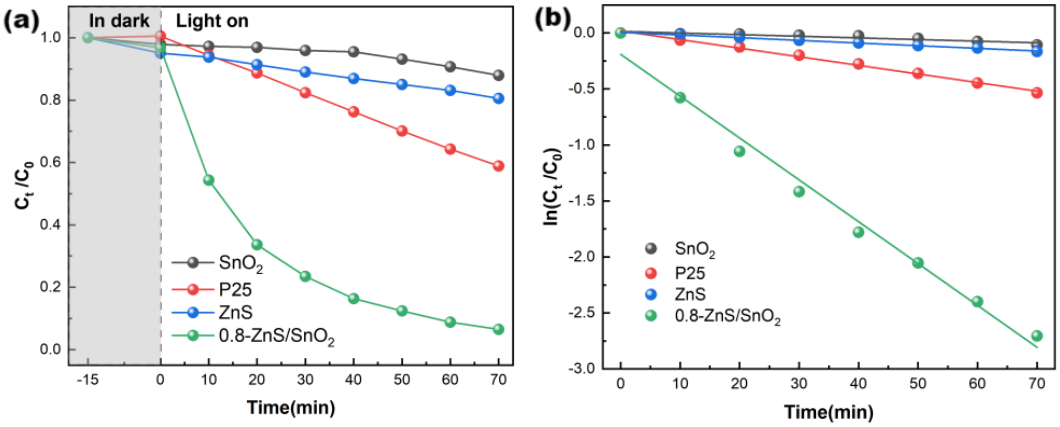

Figure 10. (a) C_t/C_0 vs. time plots for P25, SnO_2, ZnS and 0.8-ZnS/SnO_2 composite; (b) ln (C_t/C_0) vs. time plots.

After determining 0.8 as the optimal ratio for the n-ZnS/SnO_2 composite, it was compared with the single components. Commercial TiO_2 photocatalyst (P25), hydrothermally synthesized SnO_2, and hydrothermally synthesized ZnS were used for comparison. Figure 10(a) shows that compared to the commercial TiO_2 standard photocatalyst P25 (degradation efficiency 41.13% after 70 min) as well as SnO_2 and ZnS, the 0.8-ZnS/SnO_2 composite has a clear advantage, achieving a degradation rate of

93.52% in 70 min. Figure 10(b) further shows the reaction rate constants for each sample. The rate constant of P25 is only 7.68×10^{-3} min^{-1}, while that of the 0.8-ZnS/SnO_2 composite reaches 3.74×10^{-2} min^{-1}, indicating that the photocatalytic activity is nearly 5 times that of P25. This demonstrates that the prepared composite photocatalyst has much stronger photocatalytic activity than traditional P25, mainly due to the addition of ZnS, which expands the light absorption range of the composite, and the better light absorption performance enables it to perform better in the photocatalytic system.

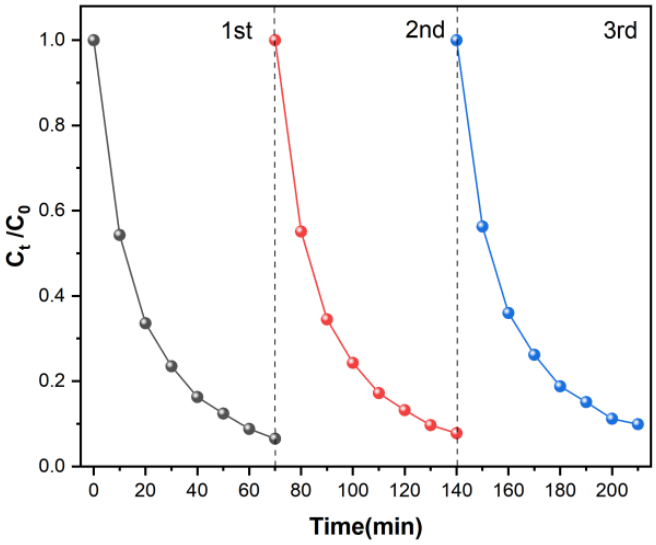

Figure 11. Cyclic catalytic test of 0.8-ZnS/SnO_2 composite.

To study the reusability and stability of the photocatalyst, repeated photocatalytic degradation tests were performed on the optimal sample, as shown in Fig. 11. For each test, 100 mg of photocatalyst was used in 100 mL of RhB solution. After three cycles, the degradation extents were almost consistent. Analysis of the test results reveals that with increasing cycle number, the photocatalytic efficiency decreases slightly: in the first cycle, the degradation efficiency reached 93.5% after 70 min; in the second cycle, it was 92.2%; in the third cycle, it was 90.1%. After 70 min of continuous degradation, the degradation efficiency remained above 90% in all cycles. During the cyclic catalytic process, the efficiency decreases somewhat, but considering that by the third cycle the sample had been continuously working in water for more than 3 hours, and that a certain amount of photocatalyst is lost during the cyclic operation, the decrease in efficiency is attributed partly to the continuous operation of the catalyst causing a reduction in its intrinsic efficiency, and partly to the unique adsorption properties of the catalyst itself, which prevent it from fully exerting its performance during recycling. Overall, since the photocatalytic degradation efficiency remains above 90% after 70 min in each cycle, it fully demonstrates the reusability and photocatalytic stability of the prepared heterojunction material.

4. CONCLUSION

In this paper, a ZnS/SnO_2 heterojunction photocatalyst was successfully prepared, with each phase maintaining its crystal structure and forming a close interface contact. The composite exhibits a mesoporous structure with a large specific surface area, which is beneficial for adsorption and photocatalytic reactions. XPS binding energy shifts confirm the directional electron transfer from ZnS to SnO_2, consistent with the type II heterojunction mechanism. The 0.8-ZnS/SnO_2 composite shows the best photocatalytic activity, with a degradation rate of 93.52% and a rate constant 5 times that of P25. The degradation rate remains above 90% after three cycles, indicating good material stability.

REFERENCES

[1] Isac, L., & Enesca, A. (2022). Recent developments in ZnS-based nanostructures photocatalysts for wastewater treatment. International Journal of Molecular Sciences, 23(24), 15668. https://doi.org/10.3390/ijms232415668

[2] Zhang, J., Qi, K., Pitcheri, R., & Duan, C. (2025). Engineering ZnS quantum dots for photocatalysis: Synthesis, modifications, and multifunctional applications. Journal of Photochemistry and Photobiology C: Photochemistry Reviews, 65, 100722. https://doi.org/10.1016/j.jphotochemrev.2025.100722

[3] Mahdizadeh, R., Sangpour, P., & Emrooz, H. B. M. (2025). Surface texture dependency of photocatalytic behavior of facile synthesized mesoporous ZnS-ZnO heterostructure under LED illumination. Scientific Reports, 15, 30272. https://doi.org/10.1038/s41598-025-94826-8

[4] (2024). Evaluation of zinc sulfide heterostructures as catalysts for the transformation of CO_2 into valuable chemicals and clean energy generation. Energy Advances, 3, 1196–1221. https://doi.org/10.1039/D4YA00287A

[5] Chatterjee, A., Kumar, G. K., Roymahapatra, G., et al. (2024). Zinc chalcogenide nanostructures: synthesis methodologies and applications—a review. Frontiers in Nanotechnology, 6, 1433591. https://doi.org/10.3389/fnano.2024.1433591

[6] Yang, T. L., Lin, P. Y., Fu, Y. S., et al. (2025). Synthesis and photocatalytic performance of ZnS nanoparticles via electrospinning assisted hydrothermal technique. Chalcogenide Letters, 22(7), 625–636.

[7] Liu, L., Wang, L., Sun, D., et al. (2023). ZnO-ZnS heterostructure as a potent photocatalyst in the preparation of some substituted chromenes and remarkable antigastrointestinal cancer activity. ACS Omega, 8(46), 44276–44286. https://doi.org/10.1021/acsomega.3c06279

[8] Al-Mobydeen, A., AlShamaileh, E., Lahlouh, B., et al. (2025). Synthesis of ZnS nano-powders and fabrication of ZnS thin films via electron-beam evaporation: structural and optical characterization. Coatings, 15(7), 796. https://doi.org/10.3390/coatings15070796

[9] Kumar, A., Maan, D., Jain, K., Jain, S. K., & Tripathi, B. (2025). A comprehensive review on synthesis methods, photodegradation mechanisms, and diverse applications of tin oxide (SnO_2) nanoparticles. Journal of Luminescence, 288, 121584. https://doi.org/10.1016/j.jlumin.2025.121584

[10] Sadik, W., El-Demerdash, M. A., Nashed, A. W., Mostafa, A. A., & Lamie, E. (2024). Synthesis and investigation of optical properties and enhancement photocatalytic activity of TiO_2–SnO_2 semiconductor for degradation of organic compounds. Scientific Reports, 14, 27846. https://doi.org/10.1038/s41598-024-78694-9

[11] Reshma, T. S., Sahu, B. K., Panda, M., Annalekshmi, O., & Das, A. (2025). Band edge tuned SnO_2 quantum dots allowing superoxide generation for efficient organic pollutant degradation. Journal of Alloys and Compounds, 1030, 180846. https://doi.org/10.1016/j.jallcom.2025.180846

[12] Shabna, S., Sahaya Jude Dhas, S., & Biju, C. S. (2023). Potential progress in SnO_2 nanostructures for enhancing photocatalytic degradation of organic pollutants. Catalysis Communications, 177, 106642. https://doi.org/10.1016/j.catcom.2023.106642